Investigation of 3D Energetic Particle Transport Inside Quiet-Time Magnetosphere Using Particle Tracing in Global MHD Model

X. Shao[1, 2], Shing F. Fung[1], L. C. Tan[3], K. Papadopoulos[4], M. Wiltberger[5], and M. C. Fok[6]

Due to the presence of a magnetic field minimum in the outer cusp region, energetic particles drifting toward dayside may experience large scale transport toward high latitude. Some particle maybe trapped at high latitude and then be scattered back. These particle orbits are termed as Shabansky orbits [*Shabansky*, 1971]. Particle trajectories inside the magnetosphere can be grouped into three classes: bouncing around the equator (trapped), going through Shabansky orbit or being elevated at dayside, and lost. Characterizing these three types of particle trajectory and their dependence on solar wind conditions can help understand the trapping and loss of energetic particles in the radiation belt. We developed 3D test-particle tracing codes to investigate particle transport in global MHD model magnetosphere. In the code, protons are traced with full-motion and electrons are traced with guiding-center approximation. In this paper, we lay out the framework of studying the trapping and lost regions systematically and effects of the enhancement of the solar wind velocity on these regions. We derived the so-called Shabansky Orbit Accessibility Map (SOAM) for both electrons and protons to visualize the three orbital characteristic regions as a function of the particle's initial position and pitch angle inside quiet-time magnetosphere.

1. INTRODUCTION

Because of its potentially hazardous space environment effects on space systems, the radiation belt (RB) has been a key subject of studies in space physics. Understanding the transport of energetic RB particles is important in characterizing the radiation belt. In situ measurements have revealed that the cusp is a region of weak or depressed magnetic field [e.g. *Fung et al.*, 1997]. The presence of a local magnetic field minimum in the outer cusp can lead to off-equator transports along the Shabansky orbit [*Shabansky* 1971]. Therefore, particle trajectories inside the magnetosphere can be grouped into three classes: (a) bouncing around the equator (fully-trapped); (b) going through Shabansky orbit or significantly gaining latitudes on the dayside (Shabansky-orbit); and (c) being lost.

Recent studies [*Sheldon et al.*, 1998; *Chen et al.*, 1998; *Trattner et al.*, 2001] led to a controversy regarding the role of the cusp in producing radiation belt particles. *Sheldon et al.* [1998] reported the trapping of the energetic electrons (30 keV to ~2 MeV) in the outer cusp region and suggested the possible diffusive filling of the electron radiation belts from the cusp. *Chen et al.* [1998] reported cusp energetic particle (CEP) (several hundred keV ions) events and suggested that the cusp region can be a major particle

[1] Space Physics Data Facility (SPDF), NASA Goddard Space Flight Center, Greenbelt, Maryland
[2] National Research Council Research Associate Program, Washington DC
[3] QSS Inc., Greenbelt, Maryland
[4] Department of Astronomy, University of Maryland, College Park, Maryland
[5] N CAR, Boulder, Colorado
[6] Laboratory for Extraterrestrial Physics (LEP), NASA Goddard Space Flight Center, Greenbelt

The Inner Magnetosphere: Physics and Modeling
Geophysical Monograph Series 155

10.1029/155GM33

acceleration region of the magnetosphere. But, the acceleration mechanism is not identified. *Trattner et al.* [2001] provided an alternative explanation that the cusp energetic particles (up to several hundred keV ions) might be accelerated at the quasi-parallel bow shock, then transported downstream and enter the cusp along newly reconnected field lines or some other entry mechanism. For ions with energy above 150 keV/e, the magnetosphere itself might circulate these particles to the cusp through Shabansky orbit. In order to understand the populating of the cusp with energetic particles, we need first to understand the circulation of energetic particles in the magnetosphere. We intended in this paper not to discuss about the cusp or shock region acceleration, but rather to characterize the three types of trajectory of magnetospheric particles and quantify the accessibility of Shabansky orbit.

At present, a number of particle-tracing based radiation belt models exist [*Li et al.*, 1993, *Elkington et al.*, 2002]. These test particle-based radiation belt models trace particles either in an empirical magnetospheric model or in a 2D cut-plane from global MHD simulations. For relativistic electrons, off-equatorial transport was neglected. These models are not applicable to studying the accessibility of high latitude regions by magnetospheric particles. On the other hand, *Delcourt and Sauvaud* [1999] focused on the 3D transport of energetic protons in an empirical magnetic field model and demonstrated the populating of the cusp and boundary layers by energetic (hundreds of keV) equatorial particles (mainly protons). But it is not clear what the dependence on the initial launching location and pitch angle is for particles being able to access the dayside high latitude region. Therefore, we still do not have a clear picture about classifying the three types of particle trajectory.

Recently, we developed a 3D particle tracing code to trace energetic particles in Lyon-Fedder-Mobbary (LFM) global MHD model [*Fedder et al.*, 1995]. The global MHD model provides the particle tracing code with self-consistent electric and magnetic (EM) fields in the magnetosphere. In this paper, we show that by tracing a limited number of test particles from different locations and initial pitch angles, we can obtain the so-called Shabansky Orbit Accessibility Map (SOAM), with which we can study the grouping of the three types of particle trajectory. In this paper, we focused on the 3D transport of radiation belt particles inside the quiet-time magnetosphere formed with constant northward IMF.

In following sections, we first introduce our model of RB particle transport and validations of the codes. Then, using the model, three types of particle trajectory in the magnetosphere are identified for both energetic electrons and protons. SOAMs are constructed to understand the dependence of trapping, Shabansky-orbit and lost of the energetic particles on the initial launching location and pitch angle during different constant solar wind speeds.

2. SIMULATION MODELS

2.1. Overall Architecture of the Particle Transport Model

The newly developed radiation belt particle transport model utilizes the Lyon-Fedder-Mobbary (LFM) global MHD model [*Fedder et al.*, 1995] to provide EM fields in the magnetosphere and a 3D relativistic particle tracing code to study the spatial-temporal evolution of energetic RB electrons and protons in an evolving magnetosphere.

2.2. Global MHD Model

The electric and magnetic fields used to feed the 3D particle tracing code are taken from the LFM global MHD model [*Fedder et al.*, 1995; *Guzdar et al.*, 2001]. The core module of the LFM model is a three dimensional code that solves the ideal MHD equations in a conservative form. These equations are discretized and solved on a cylindrical staggered mesh, typically 60 R_E in radius and 330 R_E long, containing the solar wind and the magnetosphere. A spider web type computational grid places maximal resolution (0.2 to 0.4 R_E) on physically critical locations such as the bow-shock region and the inner magnetosphere. The code uses diffuse solar wind matching conditions along the outer edges of the computational domain. This permits time dependent solar wind parameters as input conditions. A simple supersonic outflow condition is used in the outer anti-solar boundary. The inner boundary is located on a geocentric sphere of radius 3 R_E, where the magnetospheric solution is matched to the solution of the ionospheric module. The ionospheric module represents the ionosphere and its coupling to the magnetosphere and solves a 2D height-integrated electrostatic potential equation.

2.3. 3-D Particle Tracing Models

Because the gyro-radius of energetic (a few hundred keV to MeV) electrons and protons in the Earth's magnetosphere differs by orders of magnitude, we developed different algorithms to trace motions of energetic electrons and protons. Namely, protons are traced with full motion and electrons are traced with guiding-center approximation.

2.3.1. Full momentum tracing for relativistic protons. *Delcourt and Sauvaud* [1999] show that for relativistic protons, full-momentum tracing is needed because in the compressed inner magnetotail and dayside cusp region,

the ratio between the gyro-radius of energetic (several hundred keV) protons and the gradient and curvature scale of the local magnetic field ($\varepsilon_r = \max(|\rho\nabla(\ln B)|, |\rho\hat{b} \bullet \nabla\hat{b}|)$) is large so that the magnetic moment (first adiabatic invariant) is not conserved. Typical criterion for the conservation of the first adiabatic invariant is $\varepsilon_r < 0.187$ [*Chirikov*, 1987]. For example, for a 500 keV proton with 90 degree pitch angle, the gyro-radius is about 0.32 R_E in a typical magnetic field of magnitude 50 nT at X ~ −7.5 R_E inside the magnetosphere. Local gradient scale and curvature scale can be <0.6 Re, resulting $\varepsilon_r > 0.53$ so that the magnetic moment is not conserved. Therefore, we trace the energetic proton by solving the full motion equations:

$$d(\gamma m_p \vec{V})/dt = q[\vec{E} + \vec{V} \times \vec{B}] \tag{1}$$

$$d(\gamma m_p c^2)/dt = q\vec{V} \bullet \vec{E} \tag{2}$$

where $\gamma = 1/\sqrt{1-(V/c)^2}$, $\vec{V}$ is the particle velocity.

The numerical scheme used to integrate the motion is similar to those used in particle codes [*Birdsall and Langdon*, 1991], namely a time-centered leap-frog scheme. Particle velocity ($\vec{V}^{n\pm1/2}$) is defined at half time step and particle position ($\vec{r}^{n\pm1}$) is defined at integer time step.

Let $\vec{u} = \gamma\vec{V}$ and consequently $(\gamma)^2 = 1 + (u/c)^2$, the motion equation can be written in the discretized form as

$$\vec{u}^{n+1/2} - \vec{u}^{n-1/2} = \frac{q\delta t}{m}[\vec{E}^n + \frac{1}{2\gamma^n}(\vec{u}^{n+1/2} + \vec{u}^{n-1/2}) \times \vec{B}^n] \tag{3}$$

Here, the velocity in the $\vec{V} \times \vec{B}$ term of equation (1) is treated with the Crank-Nicholson method. By rearranging Equation (3) and assuming $\vec{u}^{n-1/2}$, $\vec{E}^n$, $\vec{B}^n$, and $\gamma^{n-1/2}$ are known, we get equation (4) for $\vec{u}^{n+1/2}$:

$$\begin{aligned}(\vec{u}^{n+1/2} + (q\delta t/m)(1/2\gamma^n)\vec{B}^n \times \vec{u}^{n+1/2}) \\ = \vec{u}^{n-1/2} + (q\delta t/m)[\vec{E}^n + (1/2\gamma^n)\vec{u}^{n-1/2} \times \vec{B}^n]\end{aligned} \tag{4}$$

which can be easily solved with a linear equation solver. The particle position can be updated with $\vec{r}^{n+1} = \vec{r}^n + \vec{V}^{n+1/2}\delta t = \vec{r}^n + \vec{u}^{n+1/2}\delta t/\gamma^{n+1/2}$. The advancing time step is about 1/180 of proton gyration period.

2.3.2. Guiding-Center approximation for relativistic electrons. To trace energetic electrons using guiding-center approximation, we need to ensure that fields vary slowly in both space and time when compared to the particle's gyro-radius and gyro-period, or that the first adiabatic invariant is conserved. The MHD wave field varying time scale is on the order of second, which is much larger than the gyro-period of electrons, typically can be 0.001 second. The spatial criterion for the conservation of the first adiabatic invariant is given by $\varepsilon_r < 0.187$. As an example, the gyro-radius of MeV electron in 50 nT magnetic field is 0.015 R_E and the MHD simulation magnetic field variation scale is larger than 0.2 R_E (smallest grid resolution). This implies that in the absence of VLF higher frequency waves the first adiabatic invariant of relativistic electrons are mostly conserved in the inner magnetosphere.

The guiding-center motions of relativistic electrons are given by [*Northrop*, 1963]:

$$d(\gamma m_e \vec{V}_g)/dt = -e[\vec{E} + \vec{V}_g \times \vec{B}] - M\nabla B/\gamma \tag{5}$$

$$\frac{d(\gamma m_e c^2)}{dt} = -e\vec{V}_g \bullet \vec{E} + \frac{M}{\gamma}\frac{\partial B}{\partial t}, \tag{6}$$

where $M = P_\perp^2/(2m_e B)$ and $\gamma = 1/\sqrt{1-(V/c)^2}$. Here $\vec{V}_g$ is the electron guiding-center velocity, V is the magnitude of the electron velocity, and $P_\perp$ is the electron momentum perpendicular to the local magnetic field.

Equation (5) differs from the guiding-center motion equation presented in *Northrop* [1963] (Equation 1.12 in *Northrop* [1963]) with gamma factor being added to account for relativistic effects. As noted in *Northrop* [1963], Equation (5) is the most original guiding center motion equation. The guiding center velocity equations for parallel and perpendicular components, which consist of $\vec{E} \times \vec{B}$, gradient, curvature and parallel drift, can be derived from Equation (5) following procedures similar to those in *Northrop* [1963]. The advantage of using Equation (5) to describe the guiding center motion is that the parallel and perpendicular guiding center velocity is treated as an integrated entity and we don't need to project the velocity to the magnetic field back and forth during the calculation, which can otherwise be sources of numerical errors. Equation (6) has been averaged over electron gyro-period and is valid when $E_\perp/B << c$ (c is the speed of light), which is true for the electric field of MHD origin.

The numerical scheme used to integrate the guiding-center motion equation is again time-centered leap-frog scheme. The particle guiding-center velocity ($\vec{V}_g^{n\pm1/2}$) is defined at half time step and the particle position ($\vec{r}_g^{n\pm1}$) is defined at integer time step.

Similarly, let $\vec{u}_g = \gamma\vec{V}_g$, the guiding-center motion equation (6) can be discretized as

$$\begin{aligned}\vec{u}_g^{n+1/2} - \vec{u}_g^{n-1/2} = -(\delta t/m_e)(M/\gamma^n)\nabla B^n \\ -(e\delta t/m_e)[\vec{E}^n + (1/2\gamma^n)(\vec{u}_g^{n+1/2} + \vec{u}_g^{n-1/2}) \times \vec{B}^n]\end{aligned} \tag{7}$$

Here, the guiding velocity in the $\vec{V}_g \times \vec{B}$ term in Equation (6) is treated with Crank-Nicholson method. Rearranging Equation (11), we can get the equation about $\vec{u}_g^{n+1/2}$:

$$\vec{u}_g^{n+1/2} - (e\delta t/m_e)(1/2\gamma^n)\vec{B}^n \times \vec{u}_g^{n+1/2} = \vec{u}_g^{n-1/2} - (e\delta t/m_e)[\vec{E}^n + \frac{1}{2\gamma^n}\vec{u}_g^{n-1/2} \times \vec{B}^n] - (\delta t/m_e)(M/\gamma^n)\nabla B^n \quad (8)$$

which can be easily solved. Once $\vec{u}_g^{n+1/2}$ is solved, the particle guiding-center position can be updated with $\vec{r}_g^{n+1} = \vec{r}_g^n + \vec{V}_g^{n+1/2}\delta t = \vec{r}_g^n + \vec{u}_g^{n+1/2}\delta t/\gamma^{n+1/2}$. The advancing time step is adaptive and adjusted according to the parallel velocity along the magnetic field line.

2.3.3. Interpolation of MHD EM field and code validation. There can be two sources of error: the error originated form the numerical schemes used to integrate the particle motion equations and the error originated from further interpolation of the MHD field value to the particle location. Global MHD simulation outputs provide the EM field on the grid cells. We need to interpolate EM field to the particle location. For electric field, simple eight-point linear interpolation is used. For magnetic field, two kinds of interpolation have been tested: (a) interpolate and get the perturbed field at the particle location and then add the dipole field value back; (b) simple eight-point interpolation of the B field on the MHD grid.

Here, we present some results to benchmark the 3D particle-tracing codes. We traced particles with different initial energy, pitch angle and L, in a dipole field with no electric field. We tested the two interpolation schemes mentioned above. Scenario (a) essentially uses a smooth dipole field in our testing case and helps understand the error originated from the integration scheme. Scenario (b) is used to understand the error from the linear interpolation.

For relativistic protons, the particle motion is followed one complete circuit in local time with the full-motion tracing scheme. The error between initial and final energy is zero, as has been shown in *Birdsall and Langdon* [1991] that the tracing scheme conserves the particle energy. The relative errors between the initial and final values of the first, second adiabatic invariants are recorded. The first adiabatic invariant M is gyro-period-averaged to remove the first-order gyro-frequency variation in the instant value of M (due to the field inhomogeneity). The second adiabatic invariant is calculated with the integral $J = \oint p_{//} ds$ over full bounces during the tracing. For 90 degree pitch angle particle, we use the maximum off-equator deviation in Z as the error measure. Table 1 summarizes our results. In general, the numerical scheme of motion equation integration conserves M and J within 0.05% in scenario (a) and within 0.5% in scenario (b). Scenario (a) performs better than scenario (b).

Table 1. Relative errors with the tracing code for 20- and 500-keV **protons** with 45 and 90 degree pitch angle at L = 5 and 10 in a dipole field using interpolation scheme (a) interpolation of the perturbed field; (b) interpolation of magnetic field directly. M and J denote the first and second adiabatic invariant. Subscripts 0 and f denote the initial and final (after one orbit around the Earth) values. For 90 degree pitch angle particle, the error $|Z|_{max}$ is listed.

L	E_0 keV	Equ p. a.	$\left\|\frac{M_f - M_0}{M_0}\right\|$ in (a)	$\left\|\frac{M_f - M_0}{M_0}\right\|$ in (b)	$\left\|\frac{J_f - J_0}{J_0}\right\|$ or $\|Z\|_{max}$ in (a)	$\left\|\frac{J_f - J_0}{J_0}\right\|$ or $\|Z\|_{max}$ in (b)
5	20	90	4.4×10^{-5}	1.6×10^{-4}	10^{-9} Re	10^{-5} Re
5	20	45	2.3×10^{-6}	1.6×10^{-3}	$<10^{-6}$	4×10^{-4}
10	20	90	8.7×10^{-5}	3.9×10^{-4}	10^{-9} Re	10^{-6} Re
10	20	45	3.0×10^{-6}	4.5×10^{-3}	$<10^{-6}$	2×10^{-4}
5	500	90	1.6×10^{-6}	1.3×10^{-5}	10^{-9} Re	10^{-7} Re
5	500	45	3.4×10^{-4}	4.0×10^{-3}	6×10^{-6}	5×10^{-4}
10	500	90	$<10^{-6}$	8.8×10^{-4}	10^{-9} Re	10^{-6} Re
10	500	45	1.8×10^{-4}	1.2×10^{-3}	2×10^{-5}	3×10^{-4}

For relativistic electrons, the motion is similarly followed with the guiding-center tracing scheme (see section 2.3.2). The first adiabatic invariant is always conserved. The energy is also conserved throughout the tracing. Table 2 summarizes results. In general, the numerical scheme of integrating guiding-center motion equation conserves second adiabatic invariant J within 0.05% in scenario (a) and within 0.7% in scenario (b). Again, scenario (a) performs better than scenario (b). In actual simulations for both electrons and protons, we use the interpolation scheme (a) and only interpolate the perturbed magnetic field.

In the MHD simulation, the inner boundary is located on a geocentric sphere of radius 3 R_E. When particles go across

Table 2. Relative errors with the tracing code for 50- and 1000-keV **electrons** with 45 and 90 degree pitch angle at L = 5 and 10 in a dipole field using interpolation scheme (a) interpolation of the perturbed field; (b) interpolation of magnetic field directly. See Table 1 caption for further info.

L	E_0, keV	Equ. p. a.	$\left\|\frac{J_f - J_0}{J_0}\right\|$ or $\|Z\|_{max}$ in (a)	$\left\|\frac{J_f - J_0}{J_0}\right\|$ or $\|Z\|_{max}$ in (b)
5	50	90	6.3×10^{-8} Re	9.3×10^{-4} Re
5	50	45	$<10^{-6}$	2.8×10^{-3}
10	50	90	1.3×10^{-7} Re	6.6×10^{-5} Re
10	50	45	$<10^{-6}$	2.0×10^{-3}
5	1000	90	6.3×10^{-8} Re	1.2×10^{-4} Re
5	1000	45	$<10^{-6}$	6.3×10^{-3}
10	1000	90	1.3×10^{-8} Re	2.7×10^{-7} Re
10	1000	45	4.6×10^{-4}	6.0×10^{-4}

this boundary and enter the inner region, dipole field is switched on and the electric field is assumed to be zero. We also note that the co-rotation electric field is not included in the simulation since it has little effects on energetic particles for L > 6 regions. On the other hand, when particles are transported to the flank or magnetopause and meet the magnetic field line with invalid mirroring condition (i.e. open field lines), these particles will be transported away and hit the simulation outer boundary. When the particle exits the outer boundary, we mark the particle as being lost.

3. THREE TYPES OF PARTICLE TRAJECTORY IN THE MAGNETOSPHERE

The tracing codes were applied to identify the typical trajectories of energetic protons and electrons in a quiet-time Earth's magnetosphere. In this case, a steady state model magnetosphere is formed with a constant northward IMF = 5nT, solar wind velocity = 400 km/s, density = 5 /cc, and thermal speed = 40 km/s. The ionospheric conductivity = 5 mho. This idealized quiet-time magnetosphere has been studied by *Guzdar et al.* [2001]. Some features of the quiet-time magnetosphere are: the closed magnetotail length is around X = −38 R_E in the north-south plane; presence of cusp region reconnection consistent with *Kessel et al.* [1995]; four-cell ionospheric convection pattern consistent with *Kennel* [1985]; the ionospheric cross polar cap potential is around 8 kV; and the magnetospheric electric field is weak (<0.04 mV/m at geosynchronous orbit in the equatorial plane). The ionospheric four-cell potential pattern and the associated equipotentials in the equator simulated from the global MHD model [*Guzdar et al.*, 2001] are consistent with the empirical models based on observations [*Kennel*, 1995].

Plate 1 shows three types of trajectory, namely trapped, Shabansky-orbit, and lost, for energetic protons inside the steady state magnetosphere. The protons are launched at the night side along SM X axis. Plate 1A shows the trajectories of trapped protons. An 80 keV proton (white trace) launched from X = −6 R_E with 90 degree equatorial pitch angle drifts clockwise and remains in the equatorial plane (perturbations in Z within 0.002 R_E). The blue trace represents orbit of an 80 keV proton launched at x = −8 R_E with initial pitch angle 45 degree. It shows that the proton bounces around the equator while drifting clockwisely. Figure 1A shows conservation of the second adiabatic invariant vs. azimuthal angle along particle trajectory for protons in Plate 1A.

Plate 1B shows a 500 keV proton with 67.5 degree initial equatorial pitch angle executing the Shabansky orbit. Due to the existence of the cusp magnetic field minimum, the proton moves off toward high latitudes, instead of bouncing around the equator, and is trapped at high latitudes for a while. Then, the particle falls back to bouncing around the equator after

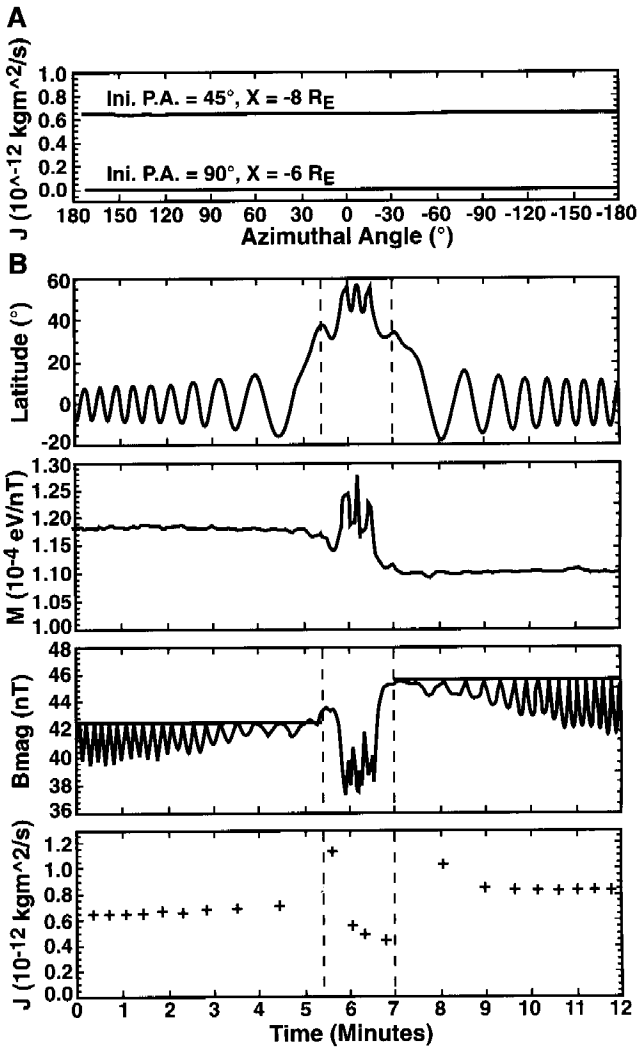

Figure 1. (A): The second adiabatic invariant vs. azimuthal angle for the trapped protons in Plate 1a. (B): Details for the particle experiencing Shabansky orbit in Plate 1b. In (B), top panel shows the evolution of the gyro-phase averaged latitude along the particle trajectory; second panel shows the gyro-phase averaged first adiabatic invariant along the particle trajectory; third panel shows the gyro-phase averaged magnetic field magnitude along the particle trajectory; bottom panel shows the second adiabatic invariant vs. time.

passing the dayside sector. To have a better understanding about the details of the proton executing Shabansky orbit, the evolutions of the first and second adiabatic invariants are shown in Figure 1B. The top panel in Figure 1B shows the evolution of the gyro-phase averaged latitude along the particle trajectory. The vertical dashed lines indicate when the particle goes through high-latitude region. The second panel in Figure 1B shows the evolution of the first adiabatic invariant M. The first adiabatic invariant is again gyro-phase averaged.

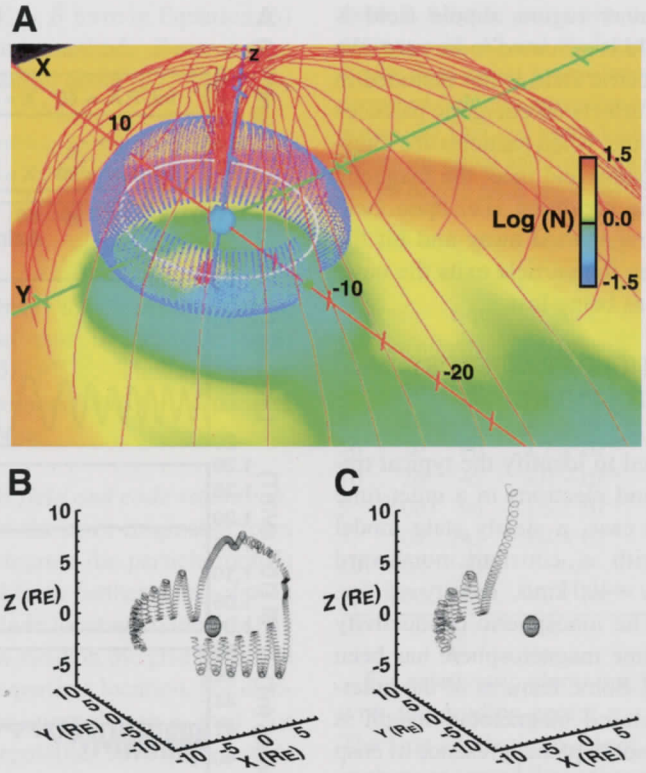

Plate 1. Three types of proton motion trace in steady state magnetosphere with northward IMF. The protons are launched at the night side along SM X axis. (A) White trace: orbit of an 80 keV proton launched from X = −6 Re with pitch angle = 90 degree. Blue trace: orbit of an 80 keV proton launched at x = −8 Re with pitch angle = 45 degree. The background is the log of the density on the Z = −5 R_E plane. The red lines are the last closed field lines of the magnetosphere. The X, Y, and Z axis' are in SM coordinate. Ticks on the axis are 5 Re apart. (B) 500 keV proton trajectory launched at X = −10.0 Re with pitch angle = 67.5 degree, showing that the proton experiences Shabansky orbit. (C) 500 keV proton trajectory launched at X = −11.6 Re with pitch angle = 75 degree, showing the proton being lost.

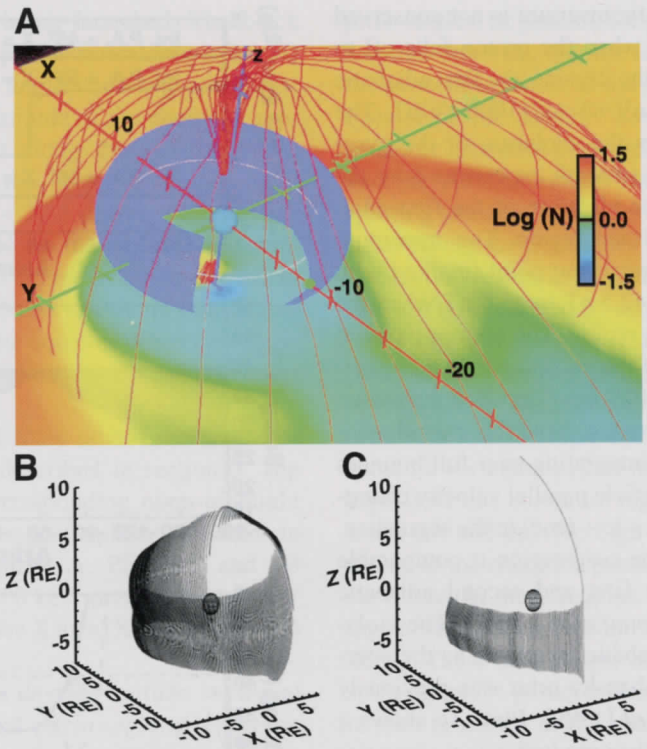

Plate 2. Typical trajectories for 1 MeV electrons launched from the night side inside a steady state magnetosphere. (A) Blue trace: orbit of 1 MeV electron launched at X = −8 R_E, pitch angle = 45 degree. White trace: orbit of 1 MeV electron launched at X = −6 R_E, pitch angle = 90 degree. The red lines, background and axis's are defined the same as those in Plate 1a. (B) electron launched at X = −11.0 Re, pitch angle = 55 degree, showing that the electron experiences Shanbansky orbit. (C) electron launched at X = −12.1 Re, pitch angle = 65 degree, showing the electron being lost.

We can see that the first adiabatic invariant is not conserved at the high latitude region and when the proton falls off to bouncing around the equator at the dayside, the first adiabatic invariant changes from 11800 eV/nT to 11000 eV/nT. The third panel in Figure 1B shows the evolution of the gyrophase averaged magnetic field strength experienced by the proton and further illustrates the violation of the first adiabatic invariant in the high latitude region. The maximum magnetic field strength at the mirroring point (marked with horizontal lines) changes from 42.5 nT to 45.5 nT when the particle passes the high-latitude region. The bottom panel in Figure 1B shows the varying of the second adiabatic invariant (from 6.5×10^{-13} to 8.3×10^{-13} kgm^2/s) when the proton goes through the high latitude region. Note the second adiabatic invariant is calculated by integrating over full bounces which are identified with the particle parallel velocity changing from – to + (start), + to – and – to + (end) in the simulation. Since local field curvature in the cusp region is comparable to the proton gyro-radius, the first and second adiabatic invariants are not conserved [*Young et al.*, 2002]. The violation of the first and second adiabatic invariants as the energetic proton going through Shabansky orbit was previously shown by *Delcourt and Sauvaud* [1999]. Plate 1c shows a 500 keV proton trajectory experiencing loss.

Plate 2 shows three types of trajectory for RB electrons traced inside the same steady state magnetosphere. Plate 2A shows that the electrons are stably trapped around the equator and drift counter-clockwise around the Earth. Plate 2B shows the trajectory of 1MeV electron experiencing the Shabansky orbit. Plate 2C shows the trajectory of an electron being lost. Top panel of Figure 2 shows evolutions of the second adiabatic invariant for the trapped electrons in Plate 2A and the Shabansky-orbit electron in Plate 2B. For the trapped electrons, the second adiabatic invariant is conserved. For the Shabansky-orbit electron, the second adiabatic invariant changes to a lower value in the high latitude region and returns to initial value after falling back to bouncing around the equator at the dayside. In the guiding-center tracing, the first adiabatic invariant is conserved and the maximum magnetic field magnitude along the particle trajectory should be constant. This is illustrated in the second panel of Figure 2. To understand the origin of the Shabansky orbit, the magnetic field magnitude along two magnetic field lines threading through the electron trajectory are plotted in the bottom panel of Figure 2. The electron is originally trapped around the equator in the potential well formed on the field line (1). The appearance of two field-strength minimums along the field line (2) and the increased equatorial magnetic field magnitude (larger than the field-strength at the electron mirroring point) cause the violation of the second adiabatic invariant. The electron is transported to the high latitude and trapped in the upper part of the field line (2). But, after the electron exits being trapped at the high-latitude region,

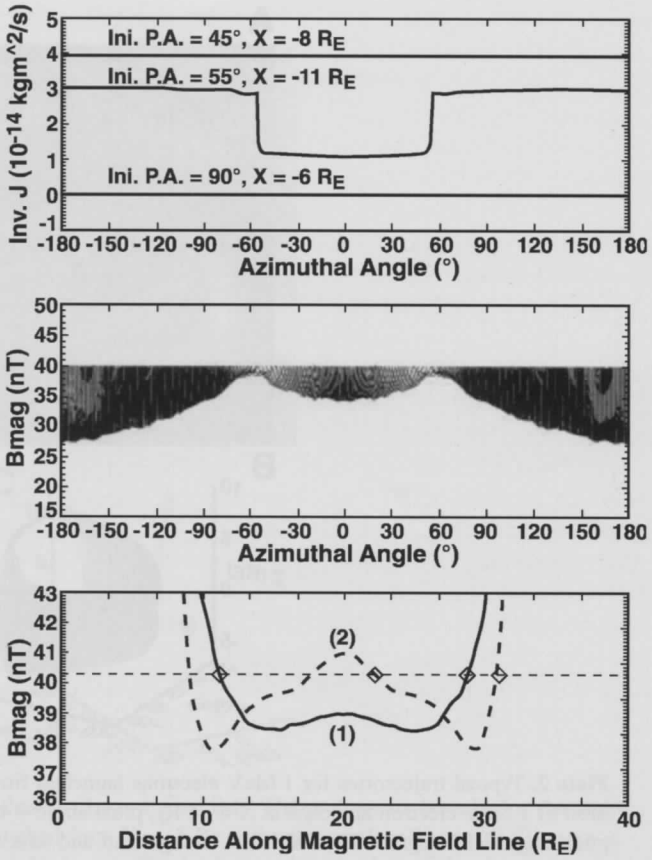

Figure 2. Top panel: the second adiabatic invariant vs. azimuthal angle for electrons in Plate 2a, b. Middle panel: The magnetic field magnitude along the trajectory of the electron experiencing Shabansky orbit (see Plate 2b). Bottom panel: showing changes in the magnetic field configuration when electron transits from being equatorially trapped to being trapped at high latitude. The magnetic field magnitude along two magnetic field lines threading through the electron trajectory are plotted. The horizontal dashed line at |B| = 40.3 nT indicates the mirroring point. Square diamonds mark mirroring points along each magnetic field line.

the second adiabatic invariant returns to its initial value. In this sense, it is conserved. These results are consistent with earlier picture depicted in *Shabansky* [1971].

4. SHABANSKY ORBIT ACCESSIBILITY MAP

By tracing particle trajectories, we can determine the fate of a particle (trapped, Shabansky-orbit, or lost) as function of initial position and equatorial pitch-angle of the particle. We introduce in this section the Shabansky Orbit Accessibility Map (SOAM) to determine the accessibility of the trapping, Shabansky-orbit and lost regions for particles originated from the tail. Plate 3A illustrates the configuration we used to derive the SOAM. In Plate 3A, pink dots along the X axis (from X = –6 to –14 Re) on the night side represent initial

positions of energetic particles being launched. The black lines on the dayside form two planar boundaries of a 3D sector (–45 degree < azimuthal angle < 45 degree), inside which we sum and average the latitude of the energetic protons. Here, 0 degree azimuth is along the sun-Earth line toward the sun. For electrons, the sector is smaller with –22.5 degree < azimuthal angle < 22.5 degree. Particles are initially launched every 0.1 R_E along the night X axis with pitch angle varying from 90 to 10 degree in 2.5 degree increment. Particles experiencing Shabansky orbit are transported either above or below the magnetic equator. When constructing the SOAM, we use the absolute value of the average latitude in the dayside sector.

We first construct the SOAM for a quiet-time magnetosphere with northward IMF as described in section 3. Top panel of Plate 3B shows the corresponding noon-midnight plane of the quiet-time model magnetosphere. We refer to this configuration as magnetosphere A. Plate 4A and 4B show SOAMs we derived for 500 keV protons and 1MeV electrons initially launched along the X axis (X = –6 to –14 Re) down the tail, respectively.

The SOAM shows the average dayside latitude vs. initial launching position and equatorial pitch angle of energetic particles. If the particle experiences bounce motion about the equator, then the average latitude = 0. The white region in the SOAM denotes the part of phase space from which particles will be lost. The colored region between the trapping and the lost region is the Shabansky-orbit region. From the SOAM, we can infer the average dayside latitude attained by a Shabansky-orbit particle. For example, a 500 keV proton launched at X = –10.1 R_E with 67.5 degree pitch angle have an average latitude of 50 degree on the dayside; a 1 MeV electron launched at X = –11.8 R_E with a pitch angle of 55 degree can have 55 degree in latitude.

We can see from Plate 4A and 4B that the overall structure of SOAMs for energetic electrons and protons are similar. Both maps show that particles with all pitch angles launched from X > –8 R_E along the tail X axis will be stably trapped around the equator. The Shabansky-orbit region has a concaved decaying slope. The general trend is that the electrons or protons launched further down the tail and with larger pitch angle are more susceptible to be transported to the Shabansky orbit on the dayside or to be lost. The initial launching position dependence of dividing the trapping, Shabansky-orbit, and lost regions can be explained by the fact that particles with same pitch angle launched further down the tail drift in larger geocentric radius and have easier access to the Shabansky -orbit or magnetopause regions. The pitch-angle dependence of dividing the three regions can be understood through the effect of drift-shell splitting according to *Roederer* [1970]. Due to the day-night asymmetry of the Earth's magnetic field, the particle drift orbits are pitch-angle dependent or disperse radially for different pitch-angles. In general, for particles launched from the same location down the tail, the larger the pitch angle the larger is the geocentric radius of the particle orbit intersected with the equator on the dayside. *Roederer* [1970] uses the first two adiabatic invariants of particles, namely the magnetic moment and the parallel motion integral, to explain the drift-shell splitting and didn't consider the effect of the Shabansky orbit. After taking the Shabansky orbit into account, there appears a transition region in SOAM. But the general trend in SOAM can still be explained by drift-shell splitting.

We can still see significant differences in fine structures between the SOAM of energetic electrons and that of protons in Plate 4A, B. The transition regions of trapping, Shabansky-orbit and lost for high energy protons in SOAM are more sporadic (or chaotic) and mixed than those of electrons. At high field line curvature regions, e.g. night side compressed inner tail and dayside high latitude cusp regions, the gyro-radius of the energetic protons is comparable to the field line curvature. In these regions, energetic protons suffer scatterings of the first and second adiabatic invariants [*Young et al.*, 2002]. These scatterings, coupled with effects of drift shell splitting, move particles chaotically to different orbits, which in turn is shown in the chaotic transition region in SOAM. Numerical discretization errors can also contribute to the complexity in the SOAM of energetic protons. On the other hand, the electron gyro-radius is much smaller than the field line curvature and transition region is smoother.

We also derived the SOAMs for protons and electrons in a more compressed magnetosphere to assess their dependences on the solar wind speed. The magnetosphere is driven with solar wind speed = 600 km/sec, IMF Bz = 5 nT and density = 5 /cc. This steady state magnetosphere is called magnetosphere B. Bottom panel of Plate 3B shows the corresponding noon-midnight plane configuration of the magnetosphere. The magnetotail in this case extends to X = –48 R_E and is more stretched. The current sheet is more compressed and moves closer to Earth. Plate 4C and 4D show the SOAMs for 500 keV protons and 1 MeV electrons, respectively. As we can see, there still exist three regions, namely trapping, Shabansky-orbit and lost regions. Higher solar wind velocity, however, causes the Shabansky-orbit region to move closer to Earth. In order to be stably trapped for all pitch angles, both electrons and protons need to be launched from X > –6.8 R_E along the tail X axis. In Plate 4C, there is a truncation region at initial launching X < –12 Re. In this region, the trapping and Shabansky-orbit regions are truncated and most protons will become lost. The appearance of the truncation region can be attributed to two factors. (1) In a more compressed tail, the cross tail drift velocity (in Y direction) of the proton is larger which moves the proton closer to the magnetopause on the flank and makes it easier to be lost. (2) in regions of high field line curvature, i.e. in a more compressed tail at midnight, the gyrophase-dependent scatterings of the first

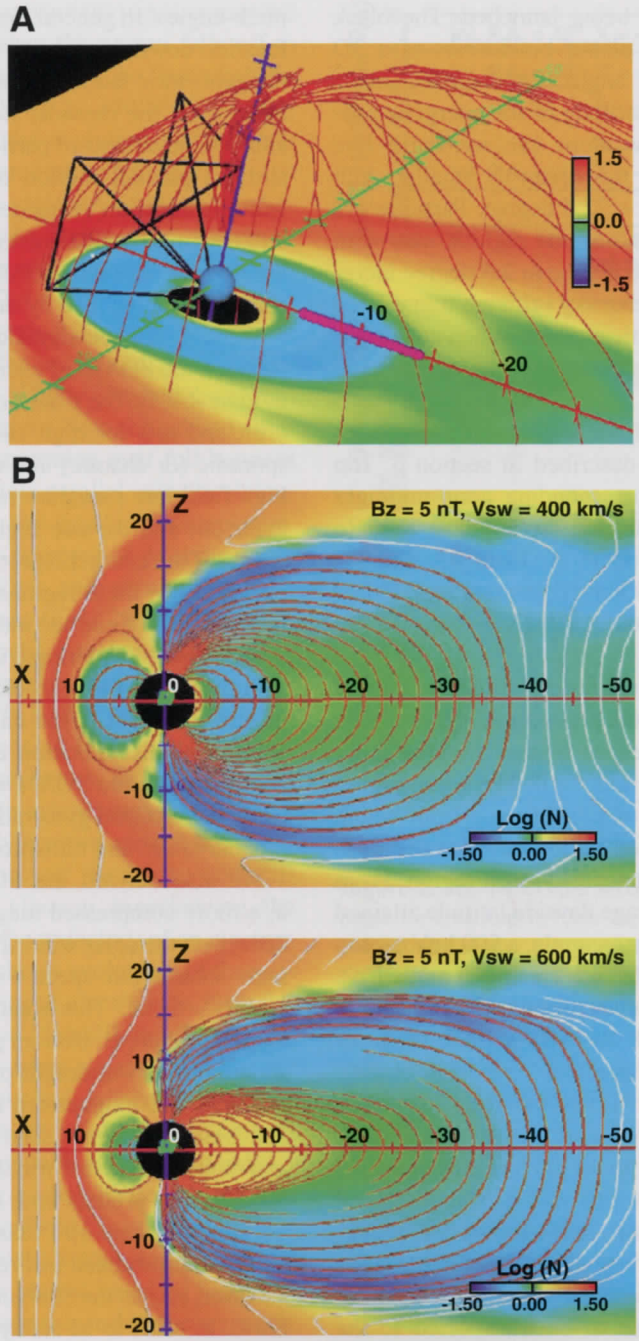

Plate 3. (A) Illustration of deriving SOAM. (B) View in the north-south plane of the magnetosphere with northward IMF. Red and white lines are the closed, open magnetic field lines, respectively. The background is the log of density. X, Z axis' point toward the sun and north, respectively. The magnetosphere is driven with northward IMF = 5 nT, and (top panel in B) velocity = 400 km/s; (bottom panel in B) velocity = 600 km/s.

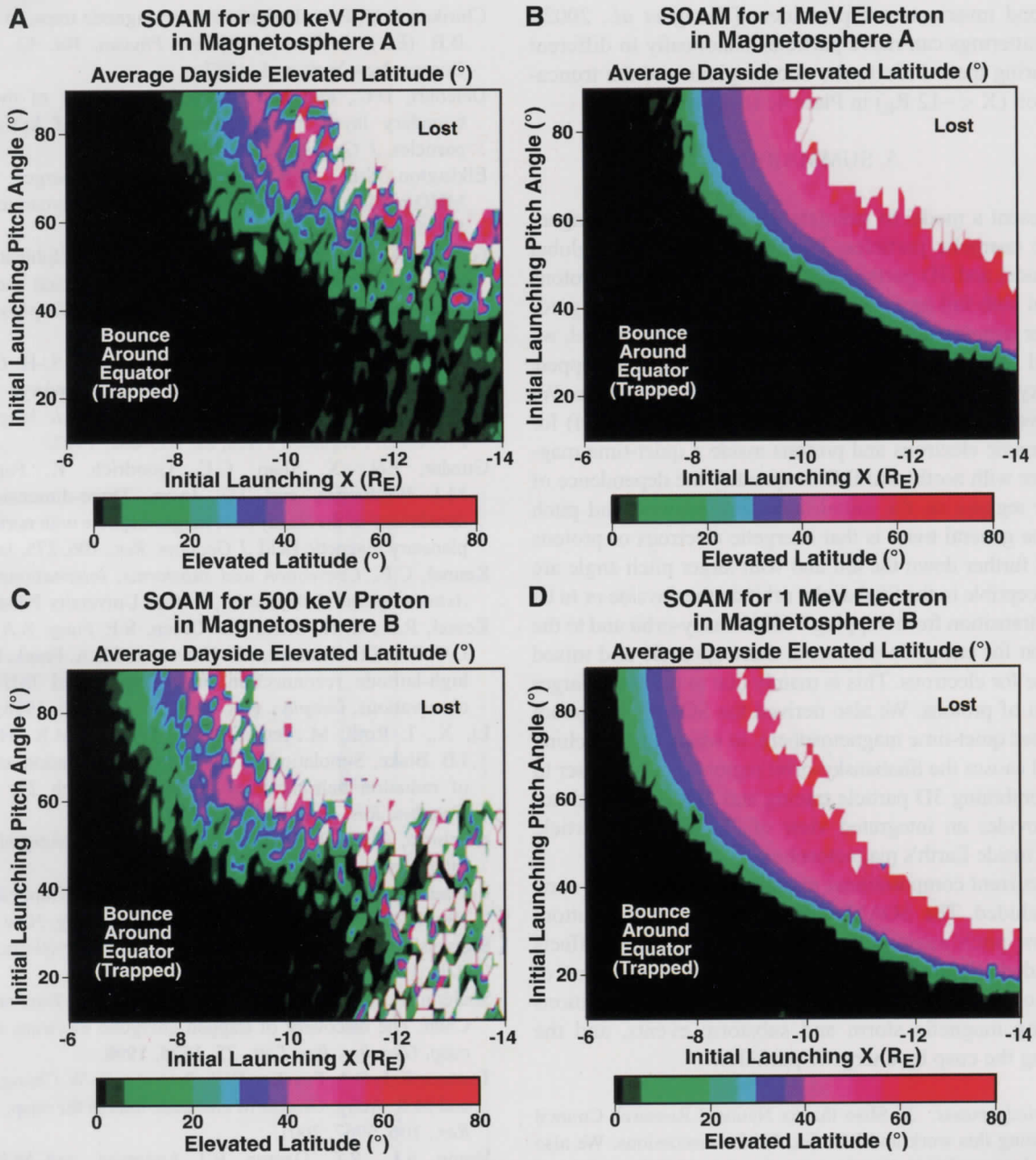

Plate 4. SOAM derived for 500 KeV protons and 1 MeV electrons in steady state magnetosphere. In all panels: the horizontal axis and vertical axis are the initial launching location down the tail and equatorial pitch angle, respectively. The color map is the average elevated latitude at the dayside. Panel (A): SOAM for 500 KeV protons and Panel (B): SOAM for 1 MeV electrons in magnetosphere A driven with SW velocity = 400 km/s (see top panel in Plate 4B); Panel (C): SOAM for 500 KeV protons and Panel (D): SOAM for 1 MeV electrons in magnetosphere B driven with SW velocity = 600 km/s (see bottom panel in Plate 4B).

and second invariants are prominent [*Young et al.*, 2002]. These scatterings can move particles chaotically to different orbits during their drifts to the noon regions and the truncation region ($X < -12\ R_E$) in Plate 4c looks mixed.

5. SUMMARY

We present a model to simulate the 3D trasport of magnetospheric energetic particles. The model combines a global MHD model and 3D particle tracing codes. Energetic protons are traced with full motion and electrons are traced with guiding-center approximation. Using the computational model, we identified three types of particle trajectory, namely trapped, Shabansky-orbit and lost, in a quiet-time magnetosphere. We also derived Shabansky Orbit Accessibility Map (SOAM) for both energetic electrons and protons inside a quiet-time magnetosphere with northward IMF to quantify the dependence of the three regions on the initial launching position and pitch angle. The general trend is that energetic electrons or protons launched further down the tail and with larger pitch angle are more susceptible to the Shabansky orbit on the dayside or to be lost. The transition from trapping to Shabansky-orbit and to the lost region for energetic protons is more sporadic and mixed than those for electrons. This is mainly due to the much larger gyro-radii of protons. We also derived the SOAMs in a more compressed quiet-time magnetosphere, in which the stretching of the tail causes the Shabansky-orbit region to move closer to Earth. Combining 3D particle tracing and global MHD simulation provides an integrated view of 3D energetic particle transport inside Earth's magnetosphere.

In the current computational model, atmospheric loss cone is not included. The SOAM will be affected in the bottom part below pitch angle = 10 degree if the loss-cone effects are included. Future work will be to study dependence of SOAMs on multi-parameters of the solar wind conditions and during magnetic storm and substorm events, and the populating the cusp by energetic particles.

Acknowledgements. X. Shao thanks National Research Council for supporting this work and P.N. Guzdar for discussions. We also thank J.G. Lyon and C.C. Goodrich for the global MHD model and discussions. Scientific computing were performed in NCSA and thunderhead cluster in NASA. This work is partially supported by NASA contract NAS 5-97059 and NASA RTOP 784-50-51-02.

REFERENCES

Birdsall, C.K. and A.B. Langdon, *Plasma Physics via Computer Simulation*, Institute of Physics Pub, 1991.

Chen, J.S., T.A. Fritz, R.B. Sheldon, H.E. Spence, W.N. Spjeldvik, J.F Fennell, S.Livi, C.T. Russell, J.S. Pickett, and D.A. Gurnett, Cusp energetic particle events: Implications for a major acceleration region of the magnetosphere, *J. Geophys. Res.*, 103, 69, 1998.

Chirikov, B.V., Particle dynamics in magnetic traps, in Kadomtsev, B.B. (Ed.), *Reviews of Plasma Physics, Vol.* 13, Consultants Bureau, New York, p. 1, 1987.

Delcourt, D.C., and J.A. Sauvaud, Populating of the cusp and boundary layers by energetic (hundreds of keV) equatorial particles, *J. Geophys. Res.*, 104, 22635, 1999.

Elkington, S.R., M.K. Hudson, M.J. Wiltberger, J.G. Lyon, MHD/particle simulations of radiation belt dynamics, *J. Atmos. Sol.-Terres. Phys.*, 64, 607, 2002.

Fedder, J.A., S.P. Slinker, J.G. Lyon, and R.D. Elphinstone, Global numerical simulation of the growth phase and the expansion onset for substorm observed by Viking, *J. Geophys. Res.*, 100, 19,083, 1995.

Fung, S.F., T.E., Eastman, S.A. Boardsen, and S.-H. Chen, High-altitude cusp positions sampled by the Hawkeye satellite, in *Proc. First Alfven Conference on Low-Latitude Magnetospheric Processes, Pergamon Press*, 22, 653-662, 1997.

Guzdar, P.N., X. Shao, C.C. Goodrich, K. Papadopoulos, M.J. Wiltberger, and J.G. Lyon, Three-dimensional MHD simulations of the steady state magnetosphere with northward interplanetary magnetic field, *J. Geophys. Res.*, 106, 275, Jan., 2001.

Kennel, C.F., *Convection and substorms*, *International Series on Astronomy and Astrophysics*, Oxford University Press, 1995.

Kessel, R.L., S.-H. Chen, J.L. Green, S.F. Fung, S.A. Boardsen, L.C. Tan, T.E. Eastman, J.D. Craven, and L.A. Frank, Evidence of high-latitude reconnection during northward IMF: Hawkeye observations, *Geophys. Res. Lett.*, 23, 583-586, 1996.

Li, X., I. Roth, M. Temerin, J.R. Wygant, M.K. Hudson, and J.B. Blake, Simulation of the prompt energization and transport of radiation belt particles during the March 24, 1991 SSC, *Geophys. Res. Lett.*, 20, 2423, 1993.

Northrop, T.G., *The adiabatic motion of charged particles*, Interscience Publishers, New York, 1963.

Roederer, J.G., Dynamics of Geomagnetically Trapped Radiation, *Physics & Chemistry in Space, Springer-Verlag*, New York, 1970.

Shabansky, V.P., Some Processes in the Magnetosphere, *Space Sci. Rev.*, 12, 299, 1971.

Sheldon, R.B., H.E. Spence, J.D. Sullivan, T.A. Fritz and Jiasheng Chen, The discovery of trapped energetic electrons in the outer cusp, *Geophys. Res. Lett.*, 25, 1825, 1998.

Trattner, K.J., S.A. Fuselier, W.K. Peterson, S.-W. Chang, R. Friedel, and M.R. Aelig, Origins of energetic ions in the cusp, J. *Geophys. Res.*, 106, 5967, 2001.

Young, S.L., R.E. Denton, B.J. Anderson, and M.K. Hudson, Emperical model for u scattering caused by field line curvature in a realistic magnetosphere, *J. Geophys. Res.*, 107, 1069, 2002.

Shing F. Fung, X. Shao, and L. C. Tan, NASA/GSFC, Code 632, Greenbelt, MD 20771, USA. (fung@mail630.gsfc.nasa.gov; shao@ mail630.gsfc.nasa.gov; ltan@mail630.gsfc.nasa.gov)

M. C. Fok, NASA/GSFC, Code 690, Greenbelt, MD, 20771, USA. (mei-ching.h.fok@nasa.gov)

K. Papadopoulos, Department of Astronomy, University of Maryland, Greenbelt, MD 20742, USA. (kp@spp.astro.umd.edu)

M. Wiltberger, NCAR, Boulder, CO 80301, USA. (wiltbemj@ucar.edu)